



Article

The “ForensOMICS” approach for postmortem interval estimation from human bone by integrating metabolomics, lipidomics and proteomics

Bonicelli, Andrea, Mickleburgh, Hayley L., Chigine, Alberto, Locci, Emanuela, Wescott, Daniel J. and Procopio, Noemi

Available at <https://clock.uclan.ac.uk/44960/>

Bonicelli, Andrea orcid iconORCID: 0000-0002-9518-584X, Mickleburgh, Hayley L., Chigine, Alberto, Locci, Emanuela, Wescott, Daniel J. and Procopio, Noemi orcid iconORCID: 0000-0002-7461-7586 (2022) The “ForensOMICS” approach for postmortem interval estimation from human bone by integrating metabolomics, lipidomics and proteomics. eLife .

It is advisable to refer to the publisher’s version if you intend to cite from the work.
<http://dx.doi.org/10.1101/2022.09.29.510059>

For more information about UCLan’s research in this area go to <http://www.uclan.ac.uk/researchgroups/> and search for <name of research Group>.

For information about Research generally at UCLan please go to <http://www.uclan.ac.uk/research/>

All outputs in CLoK are protected by Intellectual Property Rights law, including Copyright law. Copyright, IPR and Moral Rights for the works on this site are retained by the individual authors and/or other copyright owners. Terms and conditions for use of this material are defined in the [policies](#) page.

The “ForensOMICS” approach for postmortem interval estimation from human bone by integrating metabolomics, lipidomics and proteomics

Andrea Bonicelli^{1§,2}, Hayley L. Mickleburgh^{3,4}, Alberto Chighine⁵, Emanuela Locci⁵, Daniel J. Wescott⁴, Noemi Procopio^{1§,2,4*}

¹*School of Natural Sciences, University of Central Lancashire, Preston, PR1 2HE, United Kingdom*

²*The Forensic Science Unit, Faculty of Health and Life Sciences, Ellison Building, Northumbria University, Northumbria University Newcastle, Newcastle Upon Tyne, NE1 8ST, United Kingdom*

³*ACASA – Department of Archaeology, Faculty of Humanities, University of Amsterdam, PO Box 94203, 1090 GE, Amsterdam, The Netherlands*

⁴*Forensic Anthropology Center, Texas State University, San Marcos 78666, Texas, United States*

⁵*Department of Medical Science and Public Health, Section of Legal Medicine, University of Cagliari, Monserrato, 09042, Italy*

***Corresponding author:** Noemi Procopio, nprocopio@uclan.ac.uk, JB Firth Building, University of Central Lancashire, Preston, PR1 2HE, United Kingdom

§**Current address**

Abstract

The combined use of multiple omics methods to answer complex system biology questions is growing in biological and medical sciences, as the importance of studying interrelated biological processes in their entirety is increasingly recognized. We applied a combination of metabolomics, lipidomics and proteomics to human bone to investigate the potential of this multi-omics approach to estimate the time elapsed since death (*i.e.*, the postmortem interval, PMI). This “ForensOMICS” approach has the potential to improve accuracy and precision of PMI estimation of skeletonized human remains, thereby helping forensic investigators to establish the timeline of events surrounding death. Anterior midshaft tibial bone was collected from four female body donors in a fresh stage of decomposition before placement of the bodies to decompose outdoors at the human taphonomy facility managed by the Forensic Anthropological Center at Texas State (FACTS). Bone samples were again collected at selected PMIs (219, 790, 834 and 872 days). Liquid chromatography mass spectrometry (LC-MS) was used to obtain untargeted metabolomic, lipidomic and proteomic profiles from the pre- and post-placement bone samples. Univariate and multivariate analysis were used to investigate the three omics blocks independently and followed by Data Integration Analysis for Biomarker discovery using Latent variable approaches for Omics studies (DIABLO), to identify the reduced number of markers that could effectively describe postmortem changes and discriminate the individuals based on their PMI. The resulting model showed that pre-placement bone metabolome, lipidome and proteome profiles were clearly distinguishable from post-placement profiles. Metabolites associated with the pre-placement samples, suggested an extinction of the energetic metabolism and a switch towards another source of fuelling (*e.g.*, structural proteins). We were able to identify certain biomolecules from the three groups that show excellent potential for estimation of the PMI, predominantly the biomolecules from the metabolomics block. Our findings suggest that, by targeting a combination of compounds with different postmortem

46 stability, in future studies we could be able to estimate both short PMIs, by using
47 metabolites and lipids, and longer PMIs, by including more stable proteins.

48

49

50 **Key words: human bone, postmortem interval, decomposition, multi omics, metabolomics,**
51 **lipidomics, proteomics**

52 **1 Introduction**

53 The modifications that occur to the human body after death are complex and known to be
54 affected by a variety of intrinsic and extrinsic factors. The rate of decomposition can vary
55 significantly depending on the environment and even the manner of death. Nonetheless,
56 the process of decomposition has been demonstrated to be predictable, providing
57 opportunities to estimate the time elapsed since death (also known as postmortem interval,
58 PMI) based on gross morphological and/or microscopic changes to the body. Precise and
59 accurate estimation of the PMI is crucial to help establish the timeline of events surrounding
60 death and can help medicolegal investigators with the identification of the deceased and
61 can corroborate or negate other forensic evidence.

62 In the first hours after death, the body undergoes several postmortem changes, including
63 progressive cooling (*algor mortis*), increased rigidity associated with muscle stiffness (*rigor*
64 *mortis*), and pink-purplish discolouration, in light skinned individuals, caused by the lack of
65 blood circulation in and settling of blood in the lowest areas (*livor mortis*)¹⁻³. After these
66 stages, as the time since death increases, the breaking down and liquefaction of the organs
67 and other soft tissues will occur: a process referred to as putrefaction. The lack of
68 oxygenated circulation induces cellular hypoxia, leading to swelling of the cells, and
69 subsequent rupture of cell membranes and releasing of digestive enzymes. This triggers
70 autolytic digestion of the soft tissues⁴. The body becomes fully anaerobic, allowing anoxic
71 (endogenous) bacteria to proliferate and transmigrate throughout the entire body^{5,6}. The
72 activity of endogenous bacteria results in the accumulation of gases which cause bloating of
73 the soft tissues, starting in the abdomen, but also visible in the face in early
74 decomposition stages, and progressing towards the rest of the body. Colonisation of the
75 body by insects and exogenous bacteria, mostly aerobic microorganisms, contributes further
76 to the changes and reduction of the soft tissues^{7,8}. Besides these, other extrinsic factors
77 including abiotic environmental conditions (*e.g.*, humidity, temperature, sun exposition,
78 aeration, burial context) and biotic factors, such as the presence and type of
79 microorganisms, insects, and scavengers^{9,10}, will affect the rate of decomposition of the soft
80 tissues. Intrinsic factors known to affect the rate of decomposition include, among others,
81 body mass index, and antemortem and perimortem pathological conditions¹¹. Completion
82 of putrefaction and the activity of insects consuming the decomposing soft tissues, will
83 leave the remains completely, or almost completely, skeletonized, and dry.

84 The complex nature and interplay of intrinsic and extrinsic variables involved in the process
85 of decomposition, means that developing accurate and precise models for PMI estimation is
86 extremely challenging. Traditional methods of PMI estimation include calculating PMI using
87 the body temperature and ambient temperature (which relies on the predictability of *algor*
88 *mortis*, and works for short PMIs only), or the visual assessment of gross morphological
89 changes to the body to estimate a PMI range (short and longer PMIs). Since the rate of gross
90 morphological changes is variable, methods that rely on visual scoring of decomposition
91 stages suffer from issues of poor accuracy and precision. An additional problem of such
92 methods is the effect of interobserver variation on the scoring of decomposition stages. For
93 all commonly used PMI estimation methods, the accuracy and precision decreases
94 considerably as decomposition progresses, and is particularly problematic when the remains
95 are partially or completely skeletonized^{2,3}.

96 In recent years, the number of studies exploring the use of biomolecular methods of PMI
97 estimation has risen sharply, due to their potential for providing more accurate and precise
98 estimation methods based on the rates of decay of different molecules and compounds¹²⁻¹⁶.
99 Better understanding of biomolecular decomposition of bone will provide opportunities to
100 develop biomolecular methods for estimation of longer PMIs (*i.e.*, timeframes in which soft
101 tissues are unlikely to be preserved). Moreover, through the combined analysis of multiple
102 different panels of omics, greater precision and accuracy of PMI estimation can potentially
103 be achieved.

104 Biomolecular decomposition is caused by both enzymatic and microbial breakdown of large
105 molecules, resulting in the breakage of proteins into amino acids (AA), of carbohydrates into
106 more simple monosaccharides, and of lipids into simpler fatty acids chains^{17,18}. In
107 carbohydrate decomposition, the complex polysaccharides are normally broken down via
108 microbial activity into smaller units of monosaccharides. This breakdown can be achieved by
109 oxidation that produces carbon dioxide and water and can partially decompose resulting in
110 the production of organic acids and alcohols. Alternatively, the monosaccharides can be
111 degraded by fungal activity into glucuronic, citric, and oxalic acids, or by bacteria into lactic,
112 butyric, and acetic acids^{17,19}. During decay of lipids, free saturated and unsaturated fatty
113 acids are released due to hydrolysis mediated by the action of intrinsic lipases released after
114 death. These can then be converted into hydroxyl fatty acids (the main constituent of
115 adipocere) by the action of specific bacterial enzymes in humid environments, or can

116 associate with potassium and sodium ions, resulting in the formation of salts¹⁹. Protein
117 degradation is primarily an enzyme-driven process, led by the action of proteases, which
118 occurs at different rates for different proteins and tissues. Proteolytic enzymes induce the
119 hydrolytic breakdown of proteins and the production respectively of proteoses, peptones,
120 polypeptides, and finally AA, which can be further modified via deamination (production of
121 ammonia), decarboxylation (production of cadaverine, putrescine, tyramine, tryptamine,
122 indole, skatole and carbon dioxide) and desulfhydratation (production of hydro gen
123 sulphide, pyruvic acid, and thiols)^{17,19}.

124 The analysis of low molecular weight compounds and decomposition by-products is
125 becoming more popular in forensic science, particularly for the purpose of estimating the
126 PMI²⁰. Time since death was recently reported as the main variable driving modifications in
127 the metabolome occurring after death²¹ in many soft tissues and fluids, so the metabolomic
128 approach appears ideal to estimate PMI. However, the potential forensic significance of the
129 postmortem bone metabolome is as yet underexplored²². Several studies on soft tissues
130 (vitreous and aqueous humour) have examined metabolomics for the purpose of
131 determining short PMIs. Examining longer PMIs based on metabolomics analysis of humour
132 has not been possible due to evaporation and leakage through the corneal surface as time
133 since death progresses¹⁵. Girela et al.²³ reported a significant positive correlation between
134 postmortem interval and taurine, glutamate, and aspartate levels observed in vitreous
135 humour. These results were partially confirmed by Zelentsova et al.¹⁶, who found a
136 correlation between the levels of hypoxanthine, choline, creatine, betaine, glutamate, and
137 glycine and PMI. Another approach employing ¹H-NMR on aqueous humour from pig heads
138 reported taurine, choline, and succinate as major metabolites involved in the postmortem
139 modification¹⁵. The same study also showed an orthogonally constrained PLS2 (oCPLS2)
140 model showing prediction error of 59 min for PMI < 500 min, 104 min for PMI from 500 to
141 1000 min, and 118 min for PMI > 1000 min. Beside humour, muscle is one of the most
142 frequently targeted tissues in metabolomics studies focused on short PMI estimation. Pesko
143 et al.¹⁴ recently evaluated rat and human biceps femoris muscles from the same individuals
144 at different PMIs, demonstrating an increase of the abundance of several metabolites,
145 including most of those derived from the breakdown of proteins, and in particular
146 highlighting how threonine, tyrosine, and lysine show the most consistent and predictable
147 variations in relatively short PMIs. An untargeted metabolomics study on muscle tissue also

148 indicated the potential of isolating biomarkers associated with age²⁴, suggesting the
149 potential applications of metabolomics for both age-at-death (AAD) and PMI estimation.
150 To date, only three studies have used lipidomics assays for PMI estimation. Two of them
151 were conducted on muscle tissue and showed, in general, a negative correlation between
152 most lipid classes and PMI, as well as an increment in free fatty acids^{25,26}. The third study
153 applied lipidomics to trabecular bone samples from calcanei spanning a PMI of
154 approximately seven years and highlighted the presence of 76 potential N-acyl AA that
155 could be employed for PMI estimation, however their correlation with PMI has not yet been
156 fully elucidated²⁷.

157 Several studies have tried to quantify the degree of survival of proteins and the
158 accumulation of post-translational modifications (PTMs) of AA in both animal and human
159 models^{10,11,13,28,29} as well as under different conditions (*e.g.*, in aquatic environments,
160 different types of coffins, buried vs. surface)^{28–30}. The premise of these studies is that the
161 protective action of the hydroxyapatite is expected to enhance the survival of proteins,
162 allowing potential estimation of longer PMIs. Results generally showed that blood/plasma
163 and ubiquitous proteins decrease in their abundance constantly starting from the early
164 decomposition stages, whereas proteins more strongly connected to the mineral matrix
165 such as bone-specific proteins are able to survive for longer PMIs and can be useful
166 indicators for PMI estimation also in skeletonised remains. Similarly, also the accumulation
167 of specific non-enzymatic PTMs, such as deamidations, can be used as a biomarker for the
168 evaluation of the PMI in bones.

169 While many studies have applied different analytical platforms for proteomics,
170 metabolomics and lipidomics to several different matrices^{14–16,23,31–35}, relatively little is
171 known about the biomolecular decomposition of bone tissue. Moreover, while clinical
172 studies have applied multi-omics methods with some frequency, their potential for
173 development of more precise and accurate biomolecular PMI estimation methods has not
174 been explored. The present study applies, for the first time, a multi-omics approach (*i.e.*,
175 combined proteomics, metabolomics and lipidomics, defined here as the “ForensOMICS”
176 approach) to pre- and post-decomposition tibial cortical bone samples from four human
177 female body donors, to identify potential multi-omics biomarkers of time since death. The
178 multi-omics approach uses the natural differences in manner and rate of decomposition
179 between the different biomolecules (proteins, metabolites, lipids) to expand the potential

180 range of PMIs and to cross-correlate results between different sets of biomarkers to narrow
181 down PMI ranges based on the degradation of multiple biomolecules. The use a of a single
182 omics technique would not be suitable to investigate a wide range of potential PMIs.
183 Metabolites and lipids are appropriate for short PMIs while protein have been proved to be
184 stable across longer ones. Therefore, the combination of the three classes of biomolecules
185 aims to obtain ideal coverage across a wider range of PMIs. Additional advantages of the
186 combined application of these methods potentially include greater flexibility in application
187 across different environments and different postmortem treatments since the use of
188 multiple types of biomolecules and compounds increases the likelihood of retrieving
189 suitable markers for PMI estimation. The present study provides proof-of-concept for future
190 validation of the multi-omics approach on a larger number of individuals.

191 **2 Results**

192 **2.1 Single omics profile**

193 The metabolites matrices resulting from the combination of metabolomics ESI+ and ESI-
194 data were combined in a final matrix with a total of 104 identified compounds after the
195 removal of non-endogenous compounds following querying in HMDB. Furthermore, after
196 preliminary inspection via PCA, lipidomics ESI+ results were excluded due to their poor
197 contribution to a potential discriminant model. Each omics block was then evaluated
198 individually via univariate (Kruskal-Wallis and Dunn's pairwise test) and multivariate (PLS-
199 DA) analysis. The overall the Clustered Image Map (CIM) and individual plot obtained with
200 metabolomics suggested a clear separation between fresh and decomposed samples and
201 the total variance explained by the model in the first two components taken together was
202 60% (**Figure 1 – figure supplement 1**). More interestingly, increasing PMIs were found to
203 cluster progressively further away from the fresh individuals. By observing the clustering of
204 the variables in the CIM, it was clear the presence of three major behaviours: (i) reduction in
205 the intensity of compounds between the pre-deposition samples and the skeletonised ones;
206 (ii) higher intensity of compounds for the 219, 790, 843 days PMI groups; (iii) presence of
207 compounds that specifically were more intense in the 872 days PMI. Examples of these
208 behaviours can be observed in **Figure 1 – figure supplement 1**. These compounds were
209 found to be significant for Kruskal-Wallis but were only visually selected (**Figure 1 – figure
210 supplement 1**) because of their trend with PMI. However, these results were not fully
211 supported by statistical testing, as pairwise analysis mainly showed significant differences

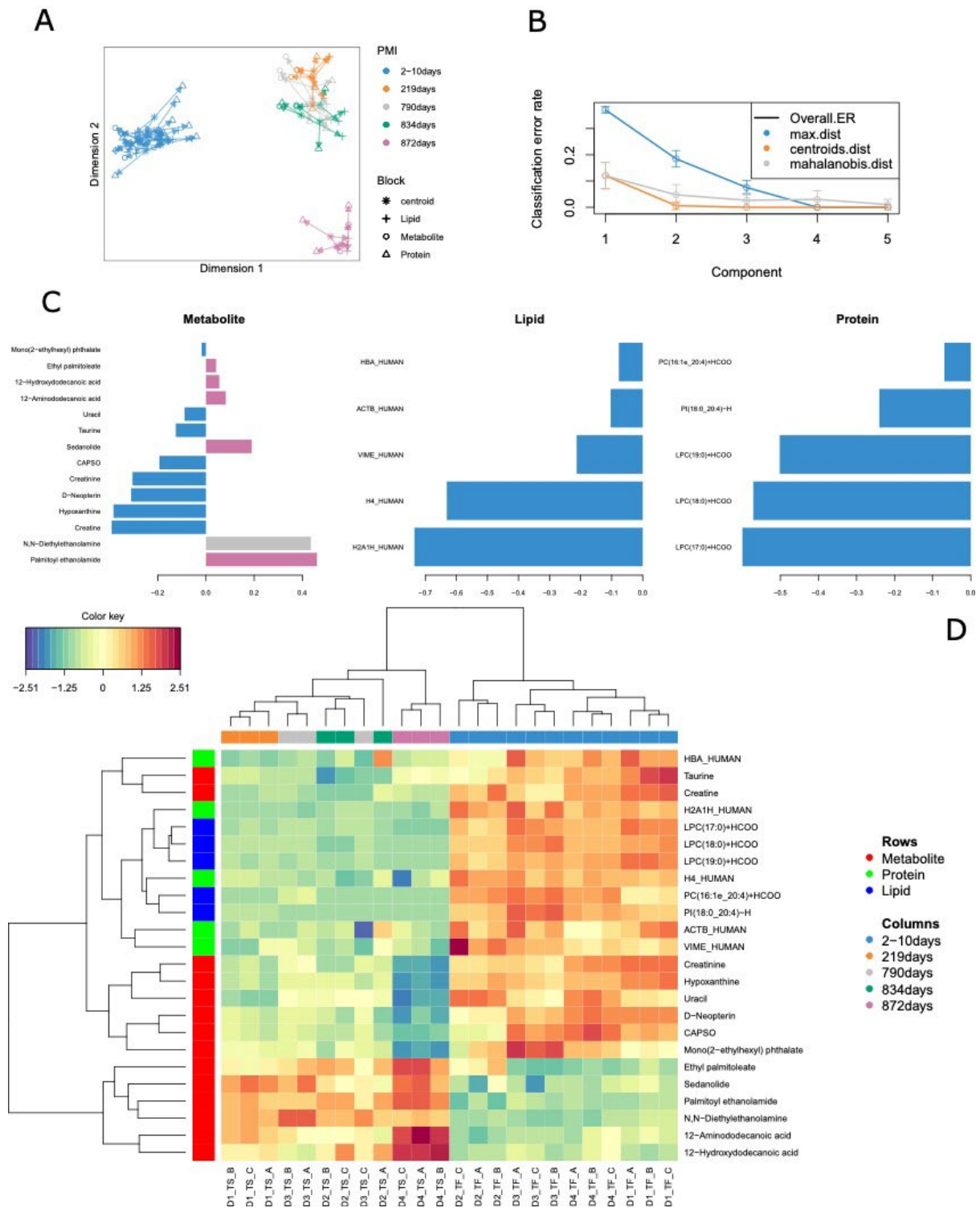
212 between few PMI groups, specifically between baseline versus more advanced PMIs (**Figure**
213 **1 – figure supplement 2**). It is interesting to note that D2 appeared to have a specific profile
214 in the pre-deposition state that clearly differed from the other donors, therefore potentially
215 affecting the overall clustering and partially hiding the effect of PMI. In contrast, D4 after
216 decomposition showed a distinct profile, likely associated with the prolonged PMI.
217 Lipidomic profiling (**Figure 1 – figure supplement 2**) showed that the closer cluster to the
218 pre-deposition individuals is the 872 days group, followed by 219, 790 and 834 days. This
219 could be related to the fact that a large number of lipids, not highly abundant in the fresh
220 portion of the sample, was found to be higher in intensity for early PMIs to then
221 progressively decrease. However, a large block constituted mostly by ceramides, was here
222 shown to be highly present in the skeletonised D4 compared to the remaining individuals,
223 suggesting a relationship with PMI. The same three behaviours extrapolated for metabolite
224 features were identified for lipids (**Figure 1 – figure supplement 2**). The model for this block
225 explains 73% of the variance in the first two components.
226 Finally, proteins showed an inferior discriminatory power in comparison with the other
227 classes of molecules according to individual consensus plot (**Figure 1 – figure supplement 3**).
228 The variance explained in the model in the first two components was only 35% and, besides
229 the major separation between pre- and post- decomposition, it was not possible to clearly
230 discriminate the various PMIs (**Figure 1 – figure supplement 3**). However, with the
231 exception of D3 (834 days PMI), it is clear that the skeletonised samples cluster away from
232 the fresh ones with increasing PMIs. Few proteins evaluated via univariate statistics,
233 however, showed clear visual and significant negative trends in the overall sample (Kruskal-
234 Wallis), although pairwise comparison could not confirm the statistical significance of the
235 difference across PMIs (Dunn’s test, **Supplementary File 1**). These proteins were
236 ASPN_HUMAN, H4_HUMAN, HBB_HUMAN, OSTP_HUMAN, VIME_HUMAN. Moreover, what
237 was clear in **Figure 1 – figure supplement 3** is the large variation between replicates that
238 could affect the evaluation of the proteins’ behaviour with PMI.

239 **2.2 Omics integration**

240 All the 24 human bone samples were included in the omics integration model (**Figure 1**). We
241 firstly evaluated correlations between the omics block using PLS regression. Results for
242 component one showed an R value of 0.94 between metabolomics and lipidomics, 0.96
243 between metabolomics and proteomics and 0.87 between lipidomics and proteomics.

244 Feature selection using the DIABLO method aimed to identify highly correlated and
245 discriminant variables across the three omics. Arrow plot (**Figure 1A**) showed the overall
246 separation between fresh and skeletonised samples, which was mainly developed along the
247 first component. However, it was possible to note that the individual with the longest PMI
248 (D4, 872 days) also clustered away from the remaining skeletonised samples along the
249 second component (**Figure 1B**). The optimal number of components was set at three by
250 means of 3-fold cross-validation repeated 100 times (**Figure 1B**). The overall balanced error
251 remained below 0.4 (**Figure 1 – figure supplement 4**). After tuning the model by attributing
252 the same weight to all the omics blocks, the ideal panel of markers selected in the first
253 component that retained most of the covariance of the system includes 14 metabolites, five
254 lipids and five proteins (**Figure 1C**). These loading plots show that a few metabolite markers
255 have a high loading for different PMIs, whereas both lipid and protein markers have high
256 values particularly for the fresh samples. Considering the individual -omics consensus plots
257 in **Figure 1 – figure supplement 5**, metabolite and lipid blocks showed a better segregation
258 between the various PMIs in the skeletonised state in comparison with the protein one.
259 There is, however, overlap in all blocks for these intermediate PMIs.

260 Multi-omics sample variations between bones from fresh and skeletonised cadavers were
261 also supported by the clustered image map (**Figure 1D**), which showed a clear separation
262 between the two groups. Most of the compounds selected by the model were highly
263 abundant in the fresh samples and less abundant in the skeletonised ones, although the
264 lower panel of metabolites (in **Figure 1D**) showed an opposite trend. In general, it could be
265 observed that the samples with shorter PMIs (up to 834 days) showed a decline for proteins,
266 lipids, and for nine of the metabolites selected for the PMI model as well as an increase in
267 the remaining seven metabolites in comparison with their fresh counterparts. Whereas the
268 decline in the abundance of proteins and lipids in comparison with the fresh samples was
269 similar between all the 12 skeletonised samples, the increase or decrease in the abundance
270 of specific metabolites was more exacerbated in the samples with the longest PMI (872
271 days) in comparison with the others (**Figure 1D**). To conclude, the model was first cross
272 validated resulting in a mean standard error of the classification error of 9.67. Additionally,
273 after performing permutation test there was still significant difference in the discrimination
274 between the PMIs ($p = 0.001$).



275

276 **Figure 1.** Results for the tuned model. (A) Arrow plot showing multiblock contexts for the
 277 overall model. (B) optimal number of components to explain model variable calculated via
 278 cross-validation. (C) Loading plot showing how each variable contribute to the covariance of
 279 each group. (D) The CIM shows the selected compounds in the final model. It is possible to
 280 see that most compounds decrease in intensity after decomposition except for few
 281 metabolites and two lipids that specifically increase in certain PMI intervals.

282

283 The following figure supplements are available for figure 1:

284
285
286
287
288
289
290
291
292
293
294
295
296
297
298
299

Figure 1 – figure supplement 1. Clustered image map (cim), sample plot and boxplot for the metabolomics data.

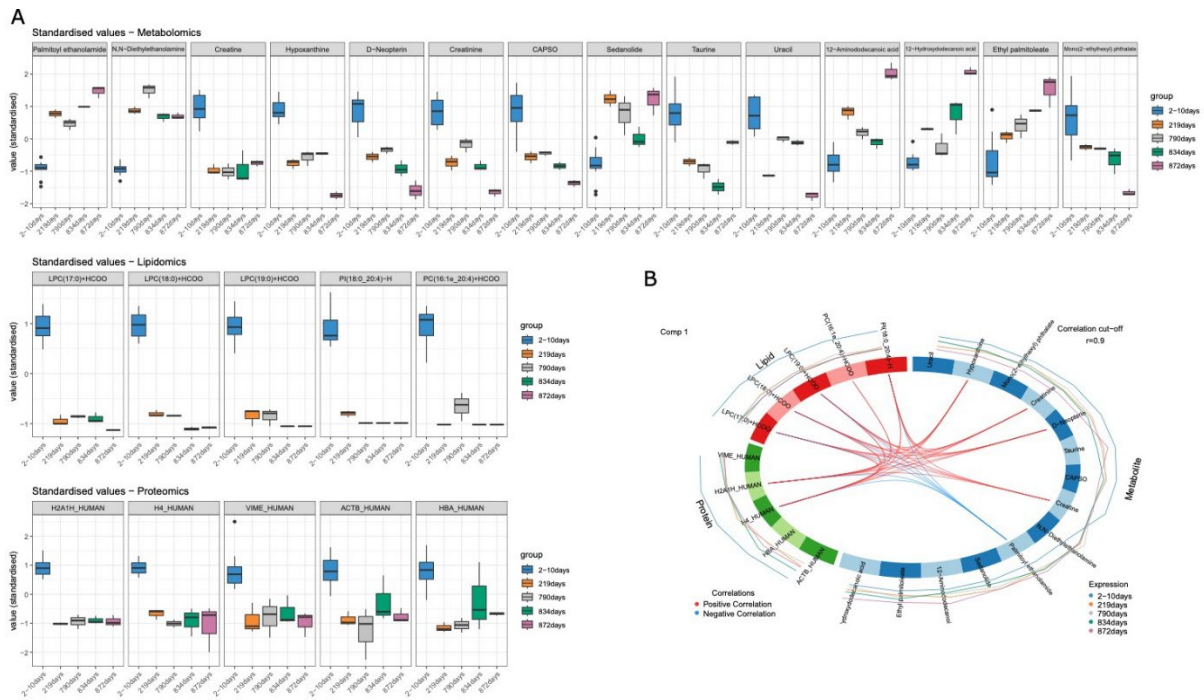
Figure 1 – figure supplement 2. Clustered image map (cim) and B) sample plot for the lipidomics data.

Figure 1 – figure supplement 3. Clustered image map (cim), sample plot and boxplot for the proteomics data.

Figure 1 – figure supplement 4. Balanced error variations across variable selection steps.

Figure 1 – figure supplement 5. Score plots for PLS-DA results of all the omics blocks considered.

300 By evaluating individual markers, it was possible to identify compounds that increased or
301 decreased consistently across the PMI (**Figure 2A**). More specifically, palmitoyl
302 ethanolamide, ethyl palmitolate, N,N-diethylethanolamine, sedanolide, 12-
303 aminododecanoic acid and acetamide showed the lowest values for the fresh samples and
304 increasing values with prolonged decomposition time. The remaining metabolites decreased
305 consistently with PMI with a considerable drop between the baseline and 219 days. Lipids
306 and proteins selected for the model, instead, were all characterised by a drastic reduction in
307 their intensity in the skeletonised samples in comparison with the fresh ones. Proteins
308 selected here were two histone proteins (histone H2A type 1-H (H2A1H), and histone H4
309 (H4)), haemoglobin subunit alpha (HBA), vimentin (VIME) and actin (ACTB).



310

311 **Figure 2.** (A) Boxplots of the selected variables after tuning that shows variation with PMI.
 312 Variables are expressed in standardised values. (B) Correlation between different omics
 313 blocks highlighting the correlations between different compounds obtained with the three
 314 omics selected in the final discriminant analysis model.

315

316 High significant correlations ($r > 0.9$) were also identified between compounds belonging to
 317 the three distinct omics blocks (**Figure 2B**). Palmitoyl ethanolamide showed negative
 318 correlation with all lipids selected but PC(16:1e_20:4)+HCOO and with H2A1H_HUMAN and
 319 H4_HUMAN proteins. Creatinine, hypoxanthine and D-Neopterin were positively correlated
 320 with all lipids selected but PC(16:1e_20:4)+HCOO and with H2A1H_HUMAN and
 321 H4_HUMAN proteins, whereas creatine was positively correlated with all lipids selected but
 322 PC(16:1e_20:4)+HCOO and with H2A1H_HUMAN.

323

324 **3 Discussion**

325 This study comprises, to the best of our knowledge, the first attempt to apply a panel of
 326 three omics methods to human bones from a controlled decomposition experiment, to
 327 identify potential biomarkers for biomolecular postmortem interval (PMI) estimation. To
 328 develop and validate multi-omics PMI estimation methods for forensic applications,
 329 replication studies in substantial sample sizes of human bones will be necessary. However,
 330 the availability of bone samples both before and after decomposition from the same
 331 individuals is currently very limited. The work presented here represents a proof-of-concept

332 study on the potential advantages of combining different omics for PMI estimation. The
333 small number of individuals included is consistent with numbers generally used in human
334 decomposition experiments, in which for practical and ethical reasons larger samples, such
335 as used in clinical studies, are very difficult to obtain. While the sample size used here is not
336 suitable for validation purposes, it serves to demonstrate the value and potential of the
337 “ForensOMICS” approach.

338 Considering each omics individually, the proteomic profile appears to show quite a
339 considerable overlap between the individuals from three post-decomposition groups (*i.e.*,
340 219, 790 and 834 days) suggesting that this method on its own does not provide sufficient
341 sensitivity to segregate close PMIs (**Figure 1 – figure supplement 3**). This could be due to the
342 nature of these biomolecules; proteins, in fact, are highly stable and may be better suitable
343 for long-term PMI estimation in forensic scenarios^{12,13} as well as in the investigation of
344 archaeological remains^{43,44}. Additionally, other analyses such as post-translational protein
345 modifications may reveal a greater potential for PMI estimation in bones than the
346 evaluation of the abundance of specific markers on their own¹². Employing a system biology
347 approach for PMI estimation for forensic purposes by combining more than one class of
348 biomolecules that have different postmortem stability¹⁷, provides a biological explanation of
349 the processes under investigation. This is achieved in this study by combining different
350 layers of omics (*i.e.*, metabolomics, lipidomics and proteomics) to reconstruct the molecular
351 profile of the overall system. The DIABLO model simultaneously identifies important
352 markers to optimise classification of PMIs by combining multiple omics techniques⁴¹. This is
353 normally used to explain the biological mechanisms that determine a disease and its
354 development, while in our case the main advantage is represented by the potential of
355 selecting a pool of compounds that effectively explains, and could accurately estimate, PMI
356 changes over an extended period of time. One interesting aspect of this approach is the
357 difference in clustering between the metabolite and lipid blocks individually compared to
358 the integration model. It can be seen in **Figure 1 – figure supplement 1** (metabolomics
359 block) that samples with increasing PMIs seems to cluster further away from the pre-
360 deposition sample in a time dependent manner, with the 219 days PMI being closer to the
361 fresh donors and the 872 days one being the furthest located. However, as suggested, the
362 metabolomics profile of D2 seems to be significantly different from the other donors in the
363 fresh state, and this could suggest that interindividual variation could affect the efficient

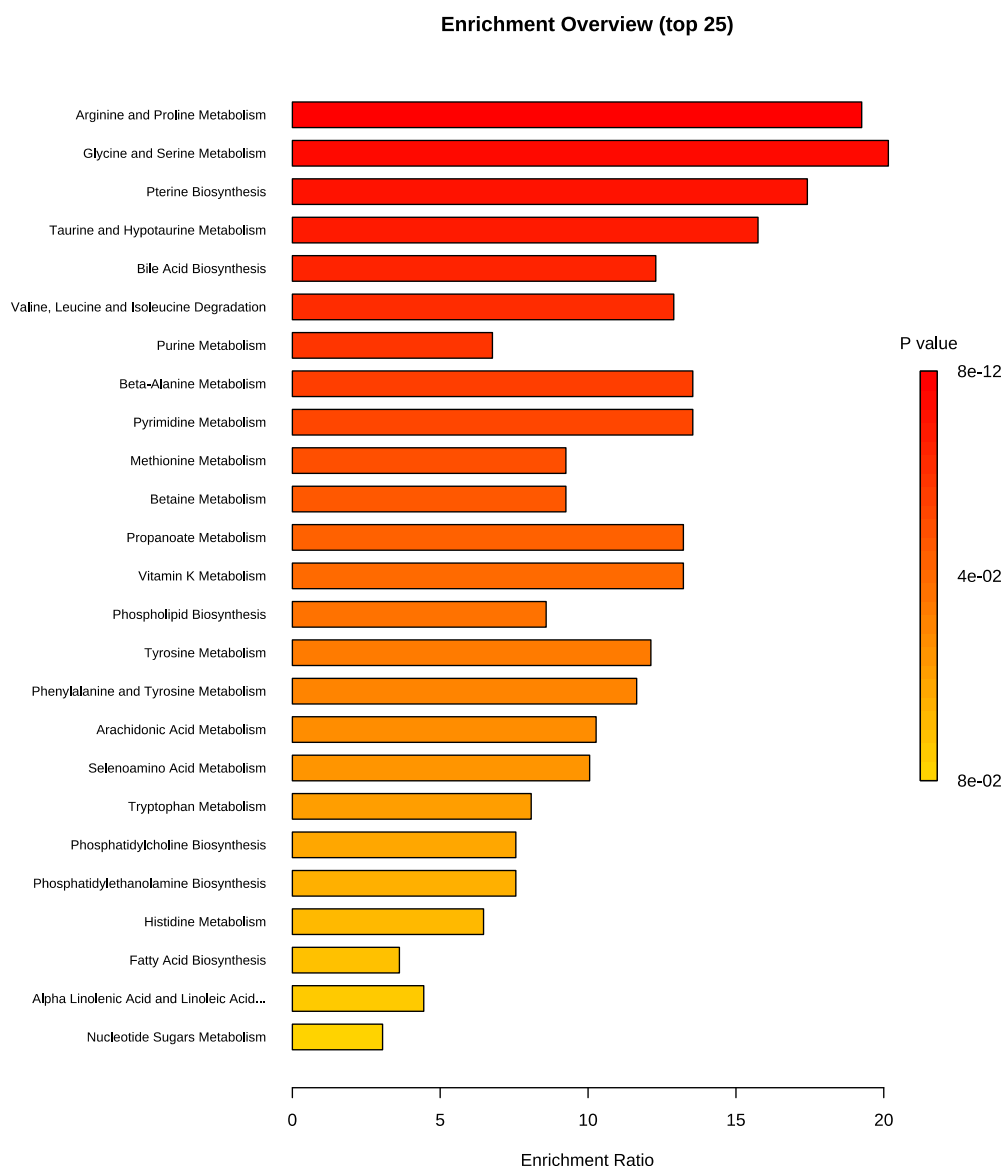
364 clustering. This has been already highlighted in the proteomics work conducted on the same
365 samples and was likely caused by the health condition of the donor prior to death¹¹. In
366 contrast, the positioning of the PMI in the cluster tree behaves in the opposite way for
367 lipids, where the various profiles seem not to be affected by any apparent interindividual
368 variation in the fresh nor in the decomposed state (**Figure 1 – figure supplement 2**).

369 Considering now the clustering of the integrative model, it provides a clear classification of
370 the PMIs obtained by the combination of the three single blocks. Since the approach chosen
371 for this pilot study was discriminant analysis and PMI was provided to the model as a
372 categorical variable, we believe that treating the response variable (PMI) as an ordinal or
373 continuous variable on a larger sample size could improve the interpretation of the results
374 and the forensic applicability of the methodology. Despite acknowledging these limitations,
375 these preliminary results show the possibility of using multiomics integration to identify
376 different PMI groups. Furthermore, the results for proteomics, that individually does not
377 allow discrimination for these specific time intervals, is integrated in the final model by
378 retaining only the proteins that contribute to PMI identification.

379 Additionally, the presence of the two main clusters identified (fresh and skeletonised) has
380 been driven by the greater differences between pre- and post-deposition. Conventionally,
381 when performing method development for PMI estimation on bone samples collections, the
382 baseline time is not available. Therefore the differences captured with the analysis would be
383 obtained on skeletonised samples only. We believe, however, that due to the uniqueness of
384 the sample it was not ideal to remove the pre-deposition specimens. Despite these issues,
385 we found moderate to high correlation between the omics blocks that allows their
386 integration using the sparse algorithm⁴¹ for PMI estimation.

387 Recently, literature has grown on the use of molecular studies via omics platforms,
388 especially for short-term PMIs. Most of the studies involving metabolomics for PMI
389 estimation focused on quickly degradable matrices (*e.g.*, muscle, blood, humour) collected
390 over a short period of time (<1 month)^{14,15,34,45,46}. As previously mentioned, the analysis of
391 proteins in bone have shown applicability to estimate relatively long PMIs in forensics^{12,29,47}
392 as well as to address archaeological questions^{48–52}, due to the prolonged survival of this type
393 of biomolecules. Finally, according to the studies presented so far, it seems that
394 postmortem changes of lipids could provide PMI estimation across several years, although
395 there is great need for validation^{27,53}. The combination of these biomolecules' classes in a

396 multi-omics model could therefore be beneficial for estimating PMI across a broader range
397 of potential PMIs. Metabolites and lipids offer accuracy in the short to medium term while
398 proteins could be the main markers for longer PMIs due to their greater stability.
399 Furthermore, variable selection^{41,42} would offer the advantage of simplifying experimental
400 procedures and targets those markers that behave consistently with PMI. To limit the
401 potential effects of interindividual variability, we considered variables that showed no
402 outliers among the four body donors and created a model that limits as much as possible
403 the number of predictors without affecting the assessment of the PMI.
404 Our results for the metabolomics assay display clear differences between the pre- and post-
405 placement bone metabolomic profiles, suggesting the potential to use these profiles to
406 assess long PMIs. The small sample size in this study does not allow us to make any deep
407 inferences about the biological significance of the metabolomics profiles of the post-
408 placement samples, as these may have been influenced by exogenous factors. With regards
409 to the pre-placement samples, the PMIs ranging between 2-10 days at 4°C would have
410 allowed some minimal postmortem modifications in the metabolome to occur²¹. The
411 metabolomic profiles of these samples are characterised by creatine, taurine, hypoxanthine,
412 3-hydroxybutyrate, creatinine, and phenylalanine. Hypoxanthine is a well-known hallmark of
413 ATP consumption and, consequently, a sign of exhaustion of normal substrates (*i.e.*, glucose
414 and pyruvate) of the Tri-Carboxylic Acid (TCA) cycle. In conjunction with the presence of
415 creatine, taurine, creatinine, phenylalanine, and 3-hydroxybutyrate, we may hypothesise a
416 switch towards TCA cycle anaplerosis through aminoacidic and ketonic substrates, in pursuit
417 of a resilient ATP production during the early/mid PMIs. Not only was the proposed
418 metabolomic approach able to identify the pre- and post-deposition groups according to the
419 bone metabolome modifications, but it was also sensitive enough to detect at very long
420 PMIs. The presence of exogenous compounds (*i.e.*, caffeine, ecgonine, dextromethorphan,
421 tramadol N-oxide, penbutolol, salicylic acid) that could reflect lifestyle habits or
422 pharmacological therapies, and thus potentially has major implications in forensic toxicology
423 and personal identification, is consistent with evidence from animal models²². Enrichment
424 analysis can be found in **Figure 3**.



425
 426 **Figure 3.** Metabolite set enrichment analysis based on differentially expressed metabolites
 427 identified in bone.
 428

429 Several polar metabolites identified in this study have previously been found in other tissues
 430 to show a consistent decay pattern after death. In fact, most of the compounds of interest
 431 matched here have already been flagged in other tissues as good potential biomarkers of
 432 PMI across shorter timeframes (**Figure 2A**). Uracil, a pyrimidine base of RNA, was previously
 433 seen to increase over a 14-day PMI in human muscle tissue when analysed by LC-MS¹⁴.
 434 Similar results for this compound were found in GC-MS analysis of rat's blood⁵⁴. In contrast,
 435 no clear association between this metabolite and PMI was found in aqueous humour¹⁵. In
 436 the present study, after a drop in normalised intestines between the baseline and first PMI,
 437 we detected an increase until 834 days, and a drop towards the longest PMI considered. It is

438 worth mentioning that most metabolites drop significantly after the baseline (“fresh”) times
439 (**Figure 2A**), suggesting that compound decomposition is driving this first part of the PMI
440 following the stop of human metabolism. It is interesting that with the increase in PMI there
441 is also an increment in several compounds that could be associated with the breakdown of
442 larger biomolecules (*e.g.*, proteins) or with the presence of microbial communities that
443 leave their own metabolic profile on bone surface. Another common marker of interest is
444 hypoxanthine for its association with hypoxia^{15,16,55–57}, that seems to drastically drop
445 between the baseline times and the first PMI timepoint, as well as in the last time interval,
446 showing a good consistency with PMI. In contrast, hypoxanthine was seen to increase until
447 48 hours and then to decrease at 72 hours in rat blood⁵⁸. Zelentsova et al.¹⁶ showed a
448 positive relation between hypoxanthine and PMI in human serum, aqueous and vitreous
449 humour. To fully understand the behaviour of this compound in bone tissue, a longitudinal
450 study should be performed also including short PMIs. Leucine has also been reported in
451 short time scale to increase in human muscle tissue¹⁴ and this agrees with our results
452 where, after the initial drop, we noticed a consistent increase from the first PMI onwards.
453 What can be clearly seen in **Figure 2A** is that D2 affects the linearity of the trend, suggesting
454 that there might be some degree of interindividual variability. This is the case for several
455 compounds; this limitation could be mitigated by increasing the number of individuals per
456 timepoint in future studies. Creatinine has previously been reported to be a good marker in
457 both muscle tissue¹⁴. Although it has not been mentioned in literature previously, we also
458 found that neopterin, a biomarker for immune system activation commonly profiled in
459 blood, serum, and urine^{59,60}, has a strong negative correlation with PMI. Taurine, also in
460 accordance with studies on vitreous humour¹⁵, showed a predictable positive behaviour
461 with PMI. Acetamide is a nitrogen-based compound associated with active and advanced
462 decay⁶¹ that, not surprisingly, showed the best positive association with PMI, resulting in
463 being the most reliable biomarker within the entire panel considered.

464 Palmitoylethanolamide is a carboximidic acid that was shown to accumulate in relation with
465 cellular stress in pig brains postmortem⁶². These findings agree with our study, which
466 revealed a clear increase of this metabolite with increasing PMIs. N,N-diethylethanolamine,
467 belonging to the class of organic compounds known as 1,2-aminoalcohols, has not yet been
468 highlighted for its potential in PMI estimation. In the current study, there is a clear increase
469 of this molecule in the decomposed samples, although no clear trends were observed across

470 the various PMIs. A proposed mechanism for its accumulation is the partial oxidation driven
471 by bacterial decomposition of monosaccharides into organic alcohols^{17,18}.

472 12-aminododecanoic acid and 12-hydroxydodecanoic acid are instead medium-chain fatty
473 acids that show a positive relationship with PMI. Previous studies based on skeletal muscle
474 tissue reported a decline in very-long-chain fatty acids^{25,26} in very short PMIs. It is not
475 possible to exclude that the cleavage of longer chains by the action of lipases or
476 microorganic activity^{17,19}. The last compound selected in the final model is methylmalonic
477 acid, a carboxylic acid which is an intermediate in the metabolism of fat and proteins. It has
478 been shown that abnormally high levels of organic acids in blood (organic acidaemia), urine
479 (organic aciduria), brain, and other tissues lead to general metabolic acidosis⁶³. In this study,
480 even with a postmortem increase in its concentration, it is not possible to identify a clear
481 trend across the decomposed samples; this may be related to inter-individual biological
482 differences of the donors involved in this study (*e.g.*, age and health condition).

483 From the lipidomic assay, only five markers were selected in the final model. These are
484 three lysophosphatidylcholines (LPCs), one phosphatidylcholine (PC) and one
485 phosphatidylinositol (PI), all showing decreasing intensities in the decomposed samples in
486 comparison with the “fresh” ones. PCs are generally the most abundant neutral
487 phospholipids and represent the main constituent in cellular membranes. LPCs are derived
488 from the hydrolysis of dietary and biliary phosphatidylcholines and are absorbed as such in
489 the intestines, but they become re-esterified before being exported in the lymph⁶⁴. They are
490 present in cell membranes and in blood. Their half-life in vivo is limited because of the quick
491 metabolic reaction that involves lysophospholipases and LPC-acyltransferases⁶⁵. In contrast,
492 PLS are amphiphilic molecules that are also minorly present in cell membranes, whose role
493 is to modulate the membrane curvature and to have other bioactive functions such as
494 interacting with peripheral proteins⁶⁶ and inhibiting osteoclast formation⁶⁷. After death,
495 these compounds can be converted into fatty acids via hydrolysis to then hydrogenise or
496 oxidase to form saturated and unsaturated fatty acids¹⁷. This process is driven by intrinsic
497 tissues lipases¹⁷. A very limited number of studies have applied lipidomics for PMI
498 estimation. Langley et al.²⁵ evaluated human skeletal muscle tissue from 31 donors over a
499 PMI of 2,000 accumulated degree days showing consistent extraction of
500 phosphatidylglycerol (PG) 34:0 and phosphatidylethanolamine (PtdE) 36:4, which showed
501 good correlation with PMI. Wood and Shirley²⁶ investigated the lipidome of human anterior

502 quadriceps muscle from one donor at 1-, 9-, and 24-day PMIs showing the decline of sterol
503 sulphates, choline plasmalogens, ethanolamine plasmalogens, and phosphatidylglycerols
504 and the increase of free fatty acids. Our results lend support to these earlier findings and
505 further confirm the potential of lipidomics for PMI estimation. Nonetheless, direct
506 comparison with these studies is not possible as they considered different tissues for much
507 shorter PMIs. Additionally, lipids profiled from the muscle tissue after decomposition are
508 suggested to derive from cell membrane breakdown^{25,26}. We suggest that, in bone material,
509 the lipidome under investigation accounts not only for cell membrane decomposition of
510 embedded osteocytes but also for the marrow and fluids embedded in the bone pores.
511 The proteomics results revealed that two ubiquitous proteins (histones), haemoglobin, actin
512 and vimentin are the best candidates within this multi-omics PMI model. These five proteins
513 selected by the model represent those which were best able to discriminate between the
514 “fresh” bones and the “skeletonised” bones but are therefore not necessarily the best
515 biomarkers to differentiate between the four post-decomposition PMIs. For insights on the
516 most suitable protein biomarkers for differentiating between the longer PMIs, identified by
517 excluding the “fresh” samples, see Mickleburgh et al.¹¹ It is not surprising to see that the
518 proteins highlighted in the model are either ubiquitous proteins or blood or muscle tissue
519 proteins, as their abundance would naturally be higher in “fresh” bone than in
520 “skeletonised” bones. The haemoglobin subunit alpha (HBA) is found in red blood cells but is
521 often also identified in bone samples with long PMIs from archaeological contexts⁶⁸, and its
522 consistent time-dependent degradation has been previously highlighted in skeletal remains
523 using several platforms^{69,70}. Furthermore, it has already been reported in skeletal tissue
524 from controlled decomposition studies of animals, and already highlighted as a potential
525 biomarker for PMI estimation¹². Vimentin (VIME) was also previously reported by Procopio
526 et al.¹² to be associated with PMI. It is a filament protein abundant in muscle tissue, and
527 therefore its association with bone, particularly with the “fresh” samples, is not unexpected.
528 However, we emphasize that this could also be due to interindividual variability, and that
529 further investigation may clarify the usefulness of VIME to estimate PMI. Actin (ACTB),
530 similar to vimentin, is a structural protein that forms cross-linked networks in the
531 cytoplasmic compartments and that is strongly connected with the presence of muscle
532 tissue residues. A previous study showed the decrease in myosin contents with increasing
533 PMIs, similarly to what we observed here for ACTB. The remaining two proteins are both

534 components of the nucleosomes, in our study were shown to be drastically reduced in bone
535 tissue also at the first the baseline PMI taken into consideration. In sum, these results
536 allowed the identification of five protein biomarkers which make good candidates for
537 estimation of short PMIs (<900 days) (*e.g.*, considering time points limited to months
538 postmortem) and not for years after death for which structural and functional proteins in
539 bone have been shown better targets to employ for PMI estimation^{11,13}.

540 Based on the findings of this exploratory study, we argue that the multi-omic method we
541 adopted here shows considerable potential for the future development of an accurate and
542 precise PMI estimation method for human bone. Further research should focus on
543 increasing the sample size, to ultimately validate the method for application in forensic
544 investigation of skeletonized human remains. Beyond the findings discussed at length
545 above, we emphasize that it is of paramount importance to establish which biomolecules
546 identified here are associated with the human metabolism and degradation, and which are
547 produced by the decomposers' microbial activity. Controlled taphonomic experiments on
548 human decomposition at human taphonomy facilities provide the opportunity to elucidate
549 biomolecular decomposition of human bone. A comprehensive understanding of the origin
550 of different compounds is key to provide a detailed explanation of the postmortem changes
551 that affect bone and other tissues, ultimately helping to shed a light on biomolecular PMI
552 investigations and on the real potential that multi-omics analyses can have in this direction.

553 **4 Materials and Methods**

554 **4.1 Body Donors**

555 Bone samples were collected from four female human body donors, aged between 61 and
556 91 years (mean 74±11.6 SD), at the Forensic Anthropology Center at Texas State University
557 (FACTS). FACTS receives whole body donations for scientific research under the Texas
558 revised Uniform Anatomical Gift Act³⁶. Body donations are made directly to FACTS and are
559 exclusively acquired through the expressed and documented will of the donors and/or their
560 legal next of kin. Demographic, health, and other information are obtained through a
561 questionnaire completed by the donor or next of kin. The data are securely curated by
562 FACTS, and the body donation program complies with all legal and ethical standards
563 associated with the use of human remains for scientific research in the United States. The
564 number of individuals (n=4) used in this preliminary study is consistent with other
565 taphonomic studies conducted on human remains for proof-of-concept purposes. Larger

566 sample sizes may be used to validate preliminary results, such as those proposed by this
567 study, at a later stage.

568 The bodies were stored in a cooler at 4°C prior to sampling. After collection of the initial
569 (pre-placement) bone samples, the bodies were placed outdoors to decompose at the
570 Forensic Anthropology Research Facility (FARF), the human taphonomy facility managed by
571 FACTS, between April 2015 and March 2018. Two of the four body donors (D1 and D4, see
572 **Table 1**), were placed in shallow hand-dug pits which were left open throughout the
573 duration of the decomposition experiment. The pits were covered with metal cages to
574 prevent disturbance by large scavengers. Donors D2 and D3 were deposited in similarly
575 sized hand-dug pits and were immediately buried with soil. Environmental data for the
576 duration of the project are available as **Supplementary File 2**.

577

Sample ID	Sex	Age (years)	PMI	Deposition context
Pre-deposition samples				
D1_TF_A	Female	91	10 days	Open pit
D1_TF_B	Female	91	10 days	Open pit
D1_TF_C	Female	91	10 days	Open pit
D2_TF_A	Female	67	2 days	Burial
D2_TF_B	Female	67	2 days	Burial
D2_TF_C	Female	67	2 days	Burial
D3_TF_A	Female	61	3 days	Burial
D3_TF_B	Female	61	3 days	Burial
D3_TF_C	Female	61	3 days	Burial
D4_TF_A	Female	77	10 days	Open pit
D4_TF_B	Female	77	10 days	Open pit
D4_TF_C	Female	77	10 days	Open pit
Post-deposition samples				
D1_TS_A	Female	91	219 days	Open pit
D1_TS_B	Female	91	219 days	Open pit
D1_TS_C	Female	91	219 days	Open pit
D2_TS_A	Female	67	834 days	Burial
D2_TS_B	Female	67	834 days	Burial
D2_TS_C	Female	67	834 days	Burial
D3_TS_A	Female	61	790 days	Burial
D3_TS_B	Female	61	790 days	Burial
D3_TS_C	Female	61	790 days	Burial
D4_TS_A	Female	77	872 days	Open pit
D4_TS_B	Female	77	872 days	Open pit
D4_TS_C	Female	77	872 days	Open pit

578

579 **Table 1.** *Sample composition, demographics, deposition context, and PMI. The Sample ID*
580 *column reports the biological replicates used. Additional information on the body donors and*
581 *observations made during collection of bone samples (e.g., medical treatments, bone colour*
582 *and density) can be found in the supplementary information in Mickleburgh et al.¹¹.*
583

584 **4.2 Sampling**

585 Bone samples (ca. 1 cm³) of the anterior midshaft tibia were collected prior to placement of
586 the body outdoors, and again upon retrieval of the completely skeletonized remains as can
587 be seen in **Figure 4**. Each body was in “fresh” stage of decomposition when pre-placement
588 samples were taken, and in “skeletonization” stage when post-placement samples were
589 collected, based on scoring of the gross morphological changes³⁷. The duration of each
590 placement and the deposition context are reported in **Table 1**. The soft tissue was incised
591 with a disposable scalpel, and a 12 V Dremel cordless lithium-ion drill with a diamond wheel
592 drill bit was used at max. 5000 revolutions to collect ~1 cm³ of bone. Sampling instruments
593 were cleaned with bleach and deionised water between each individual sample collection.
594 A total of eight samples were collected in Ziploc bags, transferred immediately to a -80°C
595 freezer, and subsequently shipped overnight on dry ice to the Forensic Science Unit at
596 Northumbria University, U.K. The samples were then transferred to a lockable freezer at -
597 20°C as per UK Human Tissue Act regulations (licence number 12495). Part of the analyses
598 were conducted by the “ForensOMICS” team (N.P. and A.B.) at Northumbria University prior
599 to their transfer to the University of Central Lancashire. Specifically, the bone samples were
600 defrosted, and fine powder was obtained with a Dremel drill equipped with diamond-tipped
601 drill bits operated at speed 5000 rpms, to avoid heat damage caused by the friction with the
602 bone. The collected powder was homogenised and stored in 2 mL protein LoBind tubes
603 (Eppendorf UK Limited, Stevenage, UK) at -80°C until extraction and testing. The powder
604 sample was later divided into 25 mg aliquots. Three biological replicates (*e.g.*, three aliquots
605 of bone sample per specimen) were extracted and analysed for each specimen. The
606 research and bone sample analyses were reviewed and approved by the Ethics committee
607 at Northumbria University (ref. 11623).



608
609
610
611

Figure 4. Positioning of the bodies in the single graves (left) pre-decomposition and (right) after complete skeletonization.

612 *The following figure supplements are available for figure 1:*

613

614 **Figure 4 – figure supplement 1.** *Flow chart of the experimental design of the study.*

615

616 **4.3 Biphasic extraction, adapted Folch protocol**

617 Chloroform (Chl), AnalaR NORMAPUR® ACS was purchased from VWR Chemicals

618 (Lutterworth, UK). Water Optima™ LC/MS Grade, Methanol (MeOH) Optima™ LC/MS Grade,

619 Pierce™ Acetonitrile (ACN), LC-MS Grade and Isopropanol (IPA), Optima™LC/MS Grade were

620 purchased from Thermo Scientific (Hemel Hempstead, United Kingdom). In total three

621 biological replicates for each of the eight specimens were extracted according to a modified

622 Folch et al.³⁸ as follow: 25mg of bone powder was placed in tube A and 750μL of 2:1 (v/v)

623 Chl:MeOH were added, vortexed for 30s and sonicated in ice for additional 20 min. 300μL of

624 LC-MS grade water was added to induce phase separation and sonicate for another 15 mins.

625 The sample were then centrifuged at 10°C for 5mins at 2000RPM. The respective upper and

626 lower fractions were collected and transferred to fresh Eppendorf tubes and the samples

627 were re-extracted with a second time using 750μL of 2:1 (v/v) Chl:MeOH. The two

628 respective fractions were combined and concentrated. The organic lipid fraction was

629 pre-concentrated using a vacuum concentrator at 55oC for 2.5 hours or until all organic

630 solvents has been removed. The aqueous metabolite fractions were flash frozen in liquid

631 nitrogen and pre-concentrated using a lyophilizer cold trap -65°C to remove all water

632 content. The respective dry fractions were then stored at -80 until analysis. The metabolite

633 fraction was resuspended in 100μL in 95:5 ACN/water (% v/v) and sonicated for 15 mins and

634 centrifuged for 15 min at 15K RPM at 4°C and supernatant was then transferred to 1.5mL

635 autosampler vials with 200μL microinsert and capped. 20μL of each sample were collected

636 and pooled to create the pooled QC. The lipid extracts were resuspended in 100μL of 1:1:2

637 (v/v) water:ACN:IPA and sonicated for sonicated for 15 min and centrifuged for 15 min at

638 15K RPM at 10oC and supernatant was then transferred to 1.5mL autosampler vials with

639 200μL microinsert and capped. 20μL of each sample were collected and pooled to create the

640 pooled QC. The sample set was then submitted for analysis.

641 **4.4 LC-MS analysis**

642 Metabolite and lipid characterization of the bone samples was performed on a Thermo

643 Scientific (Hemel Hempstead, United Kingdom) Vanquish Liquid Chromatography (LC) Front

644 end connected to IDX High Resolution Mass Spectrometer (MS) system. Full details for both
645 metabolomics and lipidomics runs are reported below.

646 **4.4.1 Metabolomics**

647 Hydrophilic Liquid Interaction Chromatography (HILIC) was used for the chromatographic
648 separation for metabolites. The separation was achieved using a Waters Acquity UPLC BEH
649 amide column (2.1 x 150mm with particle size of 1.7 μ m, part no. 186004802), operating at
650 45°C with a flow rate of 200 μ L/min. The LC gradient consists of a binary buffer system,
651 namely buffer "A" (LC/MS grade water) and buffer "B" (LC/MS grade ACN) both containing
652 10 mM ammonium formate. Independent buffer systems were used for positive and
653 negative electrospray ionisation (ESI) acquisition respectively, for ESI+ the pH of buffers was
654 adjusted using 0.1% formic acid and for negative using 0.1% ammonia solution. The LC
655 gradient was the same for both polarities, namely 95% "B" at T0 hold for 1.5min and a linear
656 decrease to 50% "B" at 11min, followed by hold for 4mins, return to starting condition and
657 hold for further 4.5 mins (column stabilization). The voltage applied for ESI+ and ESI- was
658 3.5kV and 2.5kV respectively. Injection volumes used were 5 μ L for ESI+ and 10 μ L for ESI-.

659 **4.4.2 Lipidomics**

660 Standard reverse phase chromatography was used for the chromatographic separation of
661 lipids. The separation was achieved using a Waters Acquity UPLC CSH C18 column (2.1 x
662 150mm with particle size of 1.7 μ m, part no. 186005298), operating at 55°C with a flow rate
663 of 200 μ L/min. The LC gradient consists of a binary buffer system, namely buffer "A" (LC/MS
664 grade water:ACN, 40:60 % v/v) and buffer "B" (IPA:ACN, 90:10 % v/v) both containing 10mM
665 ammonium formate. Independent buffers systems were used for positive and negative ESI
666 modes respectively, for ESI+ the pH of buffers was adjusted using 0.1% formic acid and for
667 negative using 0.1% ammonia solution. The LC gradient was the same for both polarities,
668 namely 60% "B" at T0 hold for 1.5min, linear increase to 85% "B" at 7min, increase to 95%
669 "B" at 12.5min and hold for 4.5min before returning to starting conditions and holding for
670 further 4.5min (column stabilization). The voltage applied for ESI+ and ESI- was 3.5kV and
671 2.5kV respectively. Injection volumes used were 3 μ L for ESI+ and 5 μ L for ESI-.

672 The HESI conditions for 200 μ L were as follows: sheath gas 35, auxiliary gas 7 and sweep gas
673 of 0. Ion Transfer tube temperature was set at 300°C and vaporizer temperature at 275°C.

674 These HESI conditions were applied to both metabolomics and lipidomics and lipidomics
675 assays.

676 **4.4.3 Mass spectrometry acquisition**

677 Mass spectrometry (MS) data were acquired using the AcqvieX acquisition workflow (data
678 dependent analysis). The MS operating parameters were as follows: MS1 mass resolution
679 60K, for MS2 30K, stepped energy (HCD) 20, 25, 50, scan range 100-1000, RF len (%) 35, AGC
680 gain, intensity threshold 2^4 , 25% custom injection mode with an injection time of 54 ms. An
681 extraction blank was used to create a background exclusion list and a pooled QC was used
682 to create the inclusion list.

683 **4.4.4 Data processing**

684 The metabolomic positive and negative data sets were processed via Compound
685 Discoverer™ (version 3.2) using the untargeted metabolomic workflow with precursor mass
686 tolerance 10 ppm, maximum shift 0.3min, alignment model adaptive curve, minimum
687 intensity 1^6 , S/N threshold 3, compound consolidation, mass tolerance 10 ppm, RT tolerance
688 0.3 min. Database matching were performed at MS2 level using Thermo Scientific mzCloud
689 mass spectral database with a similarity index of 50% or higher.

690 The lipidomic positive and negative data sets were processed via Thermo Scientific
691 LipidSearch™ (version 4) using the following workflow: HCD (high energy collision
692 database), retention time 0.1min, parent ion mass tolerance 5 ppm, product ion mass
693 tolerance 10ppm. Alignment method (max), top rank off, minimum m-score 5.0, all isomer
694 peaks, ID quality filter A and B only. Lipid IDs were matched using LipidSearch™ in silico
695 library at MS2 level. Corresponding metabolomics and lipidomics pooled QCs samples were
696 used to assess for instrumental drifts; the relative standard deviation (RSD) variation across
697 the QCs for metabolomics and lipidomics were less than 15%. Any metabolite/lipid feature
698 with an RSD of 25% or less within the QCs was retained.

699 **4.5 Proteomics**

700 Proteomics results from a pilot study conducted on the same samples used in this study
701 were previously published and discussed in Mickleburgh et al.¹¹. Analyses were conducted
702 following an adapted protocol developed by Procopio and Buckley³⁹ for protein extraction
703 and LC-MSMS analysis. MS data for proteomic analysis were made available via
704 ProteomeXchange Consortium via the PRIDE⁴⁰ partner repository with the data set identifier
705 PXD019693 and 10.6019/PXD019693.

706 **4.6 Statistical analysis**

707 An overview of the Forens-OMICS pipeline can be found in **Figure 4 – figure supplement 1**.
708 Metabolomics and lipidomics data were normalised by mean values, cube transformed, and
709 Pareto scaling was applied. Proteomics data were normalised using log2 transformation. For
710 preliminary data evaluation, Principal Component Analysis (PCA) was applied to the profiles
711 obtained by each single chromatography to exclude datasets with poor discriminatory
712 power. At first, univariate analysis was performed by Kruskal-Wallis. Despite the small
713 sample size per PMI, pairwise Dunn’s test with Holm’s corrected p-value was applied to the
714 set to have an overview of the differences between different PMIs. Partial Least Square
715 Discriminant Analysis (PLS-DA) was first employed to analyse each block in a multivariate
716 manner. Correlation between blocks was then investigated with pairwise PLS regression
717 prior to Data Integration Analysis for Biomarker discovery using Latent variable approaches
718 for Omics studies (DIABLO)⁴¹ based on multiblock sPLS-DA analysis using the ‘mixOmics’
719 package in R (version 4.1.2)⁴². The initial model was tuned using a 3-fold/100 repeats cross-
720 validation to perform variable selection and produce a final model that maintains the
721 maximum covariance reducing the number of the compounds used for the classification.
722 Classification error rate was further cross-validated (3-fold, 100 repeats) and significance of
723 the classification was tested via permutation test (k=3 and 999 permutation) implemented
724 in the ‘RVAideMemoire’ package⁷¹. All cross-validation in this study was performed
725 considering explicitly the biological replicates. Enrichment analysis was carried out
726 considering pre- and post-placement samples combined.

727 **5 Conclusions**

728 In conclusion, our results support the potential for developing an accurate and precise
729 multi-omics PMI estimation method for human bone for application in forensic contexts to
730 aid criminal investigation and assist with identification of the deceased. Despite the small
731 sample size used here, this study demonstrates how the approach can discriminate between
732 short- and long PMIs. This method can produce classification models including different
733 markers (*e.g.*, protein, metabolites, and lipids) to assess both short- and long-term PMIs,
734 with a high level of accuracy, as the compounds under investigation have complementary
735 decay rates. The use of different biochemical markers that have different postmortem
736 stability offers the advantage of covering both short-term PMIs, by including metabolites
737 and lipids, and long-term PMIs, by implementing in the model more stable proteins that
738 consistently degrade after death. This could not be fully proven based on our results, as the

739 PMI taken into exam is not sufficiently spread along the timeline and more individuals per
740 timepoint are necessary. However, the possibility of selecting only discriminating variables
741 allows the combination of omics that in isolation could not discriminate in a satisfactory way
742 the PMI. In the present study, proteomics did represent the less ideal omics for the
743 estimation of the time elapsed since death, however few protein variables were successfully
744 included in the model. Furthermore, in the present study the order between the various
745 PMIs was voluntarily not considered in data analysis in order to avoid biases in the
746 generation of the discriminant model. We expect that the PMI estimation over extended
747 time periods will be unlikely achieved by employing any of these three omics individually.
748 Furthermore, treating PMI as a continuous variable could be key in providing an optimal
749 approach for the estimation of PMI. Furthermore, this methodology provides new insights
750 on the biological processes that occur after death and will help establishing whether the
751 presence of certain molecules is the result of their molecular degradation or if it is mostly
752 associated with the bacterial metabolism, a central question in forensic science. The
753 proposed “ForensOMICS” approach must be validated by the analysis of substantial sample
754 sizes in future controlled taphonomic experiments conducted in multiple different
755 environments, as this represents the main source of variation in human decomposition, as
756 well as by evaluating a broader postmortem interval with a more comprehensive coverage
757 of data points in the time period taken into consideration.

758 **Acknowledgments**

759 The authors acknowledge the UKRI for supporting this work by the UKRI Future Leaders
760 Fellowship (N.P.) under grant MR/S032878/1, as well as the European Research Council (grant
761 319209) and the Leiden University Fund (grant 5604/30-4-2015/Byvanck) for supporting the
762 actualistic taphonomic experiment at FARF. We would also like to thank the NUOmics Facility
763 at Northumbria for the mass spectrometry analyses and data pre-processing, and the donors
764 and their next of kin for allowing the use of donated bodies to perform this research.

765 **Data availability**

766 This data is available at the NIH Common Fund's National Metabolomics Data Repository
767 (NMDR) website, the Metabolomics Workbench⁷² with Study ID ST002283. The data can be

768 accessed via Project DOI: 10.21228/M8MH6X. The R pipeline has been uploaded in **Source**
769 **Code File 1**.

770 Declaration of Competing interests

771 The authors have no conflict of interest to declare.

772 References

- 773 1. Clark, M. A., Worrell, M. B. & Pless, J. E. Postmortem Changes in Soft
774 Tissues. in *Forensic Taphonomy: The Postmortem Fate of Human Remains*
775 (eds. Haglund, W. D. & Sorg, M. H.) 156–164 (CRC Press, 1997).
- 776 2. Henssge, C. & Madea, B. Estimation of the time since death. *Forensic Sci Int*
777 **165**, 182–184 (2007).
- 778 3. Madea, B. Methods for determining time of death. *Forensic Sci Med Pathol* **12**,
779 451–485 (2016).
- 780 4. Goff, M. L. Early post-mortem changes and stages of decomposition in exposed
781 cadavers. *Exp Appl Acarol* **49**, 21–36 (2009).
- 782 5. Javan, G. T. *et al.* Human Thanatobiome Succession and Time since
783 Death. *Sci Rep* **6**, (2016).
- 784 6. Jans, M. M. E., Nielsen-Marsh, C. M., Smith, C. I., Collins, M. J. & Kars, H.
785 Characterisation of microbial attack on archaeological bone. *J Archaeol Sci* **31**,
786 87–95 (2004).
- 787 7. Hyde, E. R., Haarmann, D. P., Lynne, A. M., Bucheli, S. R. & Petrosino, J. F.
788 The Living Dead: Bacterial Community Structure of a Cadaver at the Onset and
789 End of the Bloat Stage of Decomposition. *PLoS One* **8**, e77733 (2013).
- 790 8. Hyde, E. R., Metcalf, J. L., Bucheli, S. R., Lynne, A. M. & Knight, R. Microbial
791 communities associated with decomposing corpses. in *Forensic Microbiology*
792 (eds. Carter, D. O., Tomberlin, J. K., Benbow, M. E. & Metcalf, J. L.) 245–273
793 (John Wiley & Sons, 2017). doi:10.1002/9781119062585.ch10.
- 794 9. Cockle, D. L. & Bell, L. S. Human decomposition and the reliability of a
795 ‘Universal’ model for post mortem interval estimations. *Forensic Sci Int* **253**,
796 136.e1-136.e9 (2015).
- 797 10. Procopio, N., Chamberlain, A. T. & Buckley, M. Intra- and Interskeletal
798 Proteome Variations in Fresh and Buried Bones. *J Proteome Res* **16**, 2016–2029
799 (2017).
- 800 11. Mickleburgh, H. L. *et al.* Human Bone Proteomes before and after
801 Decomposition: Investigating the Effects of Biological Variation and
802 Taphonomic Alteration on Bone Protein Profiles and the Implications for
803 Forensic Proteomics. *J Proteome Res* **20**, 2533–2546 (2021).
- 804 12. Procopio, N., Williams, A., Chamberlain, A. T. & Buckley, M. Forensic
805 proteomics for the evaluation of the post-mortem decay in bones. *J Proteomics*
806 **177**, 21–30 (2018).
- 807 13. Prieto-Bonete, G., Pérez-Cárceles, M. D., Maurandi-López, A., Pérez-Martínez,
808 C. & Luna, A. Association between protein profile and postmortem interval in
809 human bone remains. *J Proteomics* **192**, 54–63 (2019).
- 810 14. Pesko, B. K. *et al.* Postmortomics: The Potential of Untargeted Metabolomics to
811 Highlight Markers for Time Since Death. *OMICS* **24**, 649–659 (2020).

- 812 15. Locci, E. *et al.* A ¹H NMR metabolomic approach for the estimation of the time
813 since death using aqueous humour: an animal model. *Metabolomics* **15**, (2019).
- 814 16. Zelentsova, E. A. *et al.* Post-mortem changes in metabolomic profiles of human
815 serum, aqueous humor and vitreous humor. *Metabolomics* **16**, (2020).
- 816 17. Dent, B. B., Forbes, S. L. & Stuart, B. H. Review of human decomposition
817 processes in soil. *Environmental Geology* **45**, 576–585 (2004).
- 818 18. Nolan, A. N., Mead, R. J., Maker, G. & Speers, S. J. A review of the
819 biochemical products produced during mammalian decomposition with the
820 purpose of determining the post-mortem interval. *Australian Journal of*
821 *Forensic Sciences* **52**, 477–488 (2020).
- 822 19. Stuart B. Decomposition chemistry: overview, analysis, and interpretation. in
823 *Encyclopedia of Forensic Sciences* (eds. Siegel J A, Saukko P J & Houck M M)
824 11–15 (AcademicPress, 2013).
- 825 20. Locci, E. *et al.* Forensic NMR metabolomics: one more arrow in the quiver.
826 *Metabolomics* **16**, (2020).
- 827 21. Chighine, A., Locci, E., Nioi, M. & d’Aloja, E. Looking for Post-Mortem
828 Metabolomic Standardization: Waiting for Godot—The Importance of Post-
829 Mortem Interval in Forensic Metabolomics. *Chem Res Toxicol* **34**, 1946–1947
830 (2021).
- 831 22. Alldritt, I. *et al.* Metabolomics reveals diet-derived plant polyphenols
832 accumulate in physiological bone. *Sci Rep* **9**, 8047 (2019).
- 833 23. Girela, E. *et al.* Free amino acid concentrations in vitreous humor and
834 cerebrospinal fluid in relation to the cause of death and postmortem interval. *J*
835 *Forensic Sci* **53**, 730–733 (2008).
- 836 24. Wilkinson, D. J. *et al.* Untargeted metabolomics for uncovering biological
837 markers of human skeletal muscle ageing. *Aging* **12**, 12517–12533 (2020).
- 838 25. Langley, N., Wood, P., Herring, P. & Steadman, D. Forensic Postmortem
839 Interval Estimation from Skeletal Muscle Tissue: A Lipidomics Approach.
840 *Forensic Anthropology* **2**, (2019).
- 841 26. Wood, P. L. & Shirley, N. R. Lipidomics Analysis of Postmortem Interval:
842 Preliminary Evaluation of Human Skeletal Muscle. *Metabolomics* **3**, 1000127
843 (2013).
- 844 27. Dudzik, B., Langley, N. R., Meadows Jantz, L., Cebak, J. & Wood, P.
845 Postmortem Interval Estimation Using Bone Lipidomics. in *American Academy*
846 *of Forensic Sciences 70th Annual Scientific Meeting* (2017).
- 847 28. Procopio, N., Mein, C. A., Starace, S., Bonicelli, A. & Williams, A. Bone
848 Diagenesis in Short Timescales: Insights from an Exploratory Proteomic
849 Analysis. *Biology (Basel)* **10**, 460 (2021).
- 850 29. Mizukami, H., Hathway, B. & Procopio, N. Aquatic Decomposition of
851 Mammalian Corpses: A Forensic Proteomic Approach. *J Proteome Res* **19**,
852 2122–2135 (2020).
- 853 30. Bonicelli, A., di Nunzio, A., di Nunzio, C. & Procopio, N. Insights into the
854 Differential Preservation of Bone Proteomes in Inhumed and Entombed
855 Cadavers from Italian Forensic Caseworks. *J Proteome Res* **21**, 1285–1298
856 (2022).
- 857 31. Li, W. *et al.* Vitreous humor: A review of biochemical constituents in
858 postmortem interval estimation. *Journal of Forensic Science and Medicine* **4**, 85
859 (2018).
- 860 32. Wu, Z. *et al.* Estimation of early postmortem interval in rats by GC–MS-based
861 metabolomics. *Leg Med* **31**, 42–48 (2018).

- 862 33. Hirakawa, K. *et al.* Experimental estimation of postmortem interval using
863 multivariate analysis of proton NMR metabolomic data. *Leg Med* **11**, (2009).
- 864 34. Banaschak, S., Rzanny, R., Reichenbach, J. R., Kaiser, W. A. & Klein, A.
865 Estimation of postmortem metabolic changes in porcine brain tissue using 1H-
866 MR spectroscopy - Preliminary results. *Int J Legal Med* **119**, 77–79 (2005).
- 867 35. Li, C. *et al.* MALDI-TOF MS as a Novel Tool for the Estimation of Postmortem
868 Interval in Liver Tissue Samples. *Sci Rep* **7**, 1–11 (2017).
- 869 36. *Death and Disposition of the Body, Disposition of the Body, Revised Uniform*
870 *Anatomical Gift Act. Health and Safety Code*
871 (<https://statutes.capitol.texas.gov/Docs/HS/htm/HS.692A.htm>, 2009).
- 872 37. Megyesi, M. S., Nawrocki, S. P. & Haskell, N. H. Using accumulated degree-
873 days to estimate the postmortem interval from decomposed human remains. *J*
874 *Forensic Sci* **50**, 618–26 (2005).
- 875 38. Folch, J., Lees, M. & Sloane Stanley, G. H. A simple method for the isolation
876 and purification of total lipides from animal tissues. *J Biol Chem* **226**, 497–509
877 (1957).
- 878 39. Procopio, N. & Buckley, M. Minimizing Laboratory-Induced Decay in Bone
879 Proteomics. *J Proteome Res* **16**, 447–458 (2017).
- 880 40. Ternent, T. *et al.* How to submit MS proteomics data to ProteomeXchange via
881 the PRIDE database. *Proteomics* **14**, 2233–2241 (2014).
- 882 41. Singh, A. *et al.* DIABLO: an integrative approach for identifying key molecular
883 drivers from multi-omics assays. *Bioinformatics* **35**, 3055–3062 (2019).
- 884 42. Rohart, F., Gautier, B., Singh, A. & Lê Cao, K.-A. mixOmics: An R package for
885 ‘omics feature selection and multiple data integration. *PLoS Comput Biol* **13**,
886 e1005752 (2017).
- 887 43. Wadsworth, C. *et al.* Comparing ancient DNA survival and proteome content in
888 69 archaeological cattle tooth and bone samples from multiple European sites. *J*
889 *Proteomics* **158**, 1–8 (2017).
- 890 44. Warinner, C., Korzow Richter, K. & J. Collins, M. Paleoproteomics. *Chem Rev*
891 **0**, (2022).
- 892 45. Ith, M. *et al.* Estimation of the postmortem interval by means of 1H MRS of
893 decomposing brain tissue: Influence of ambient temperature. *NMR Biomed* **24**,
894 791–798 (2011).
- 895 46. Ith, M. *et al.* Observation and identification of metabolites emerging during
896 postmortem decomposition of brain tissue by means of in situ 1H-magnetic
897 resonance spectroscopy. *Magn Reson Med* **48**, 915–920 (2002).
- 898 47. Procopio, N., Chamberlain, A. T. & Buckley, M. Exploring Biological and
899 Geological Age-related Changes through Variations in Intra- and Intertooth
900 Proteomes of Ancient Dentine. *J Proteome Res* **17**, 1000–1013 (2018).
- 901 48. Ntasi, G. *et al.* Molecular signatures written in bone proteins of 79 AD victims
902 from Herculaneum and Pompeii. *Sci Rep* **12**, 8401 (2022).
- 903 49. Pal Chowdhury, M. *et al.* Machine learning ATR-FTIR spectroscopy data for
904 the screening of collagen for ZooMS analysis and mtDNA in archaeological
905 bone. *J Archaeol Sci* **126**, (2021).
- 906 50. Brandt, L. Ø. & Mannering, U. Taxonomic identification of Danish Viking Age
907 shoes and skin objects by ZooMS (Zooarchaeology by mass spectrometry). *J*
908 *Proteomics* **231**, (2021).
- 909 51. Richter, K. K., Codlin, M. C., Seabrook, M. & Warinner, C. A primer for
910 ZooMS applications in archaeology. *Proceedings of the National Academy of*
911 *Sciences* **119**, (2022).

- 912 52. Brown, S. *et al.* Identification of a new hominin bone from Denisova Cave,
913 Siberia using collagen fingerprinting and mitochondrial DNA analysis. *Sci Rep*
914 **6**, 1–8 (2016).
- 915 53. Dudzik, B., Jantz, L. M., Langley, N. R. & Wood, P. Postmortem Interval
916 Determination from Bone: A Metabolomics and Lipidomics Approach. *NIJ*
917 *report 304294* (2020).
- 918 54. Dai, X. *et al.* An experimental study on investigating the postmortem interval in
919 dichlorvos poisoned rats by GC/MS-based metabolomics. *Leg Med* **36**, 28–36
920 (2019).
- 921 55. Kaszynski, R. H. *et al.* Postmortem interval estimation: a novel approach
922 utilizing gas chromatography/mass spectrometry-based biochemical profiling.
923 *Anal Bioanal Chem* **408**, 3103–3112 (2016).
- 924 56. Jawor, P. *et al.* Metabolomic studies as a tool for determining the post-mortem
925 interval (PMI) in stillborn calves. *BMC Vet Res* **15**, (2019).
- 926 57. Locci, E. *et al.* Comparative use of aqueous humour ¹H NMR metabolomics
927 and potassium concentration for PMI estimation in an animal model. *Int J Legal*
928 *Med* **135**, 845–852 (2021).
- 929 58. Donaldson, A. E. & Lamont, I. L. Biochemistry changes that occur after death:
930 Potential markers for determining post-mortem interval. *PLoS One* **8**, (2013).
- 931 59. Melichar, B. *et al.* Neopterin as a biomarker of immune response in cancer
932 patients. *Ann Transl Med* **5**, 280–280 (2017).
- 933 60. Laudanski, K. *et al.* Longitudinal urinary biomarkers of immunological
934 activation in covid-19 patients without clinically apparent kidney disease versus
935 acute and chronic failure. *Sci Rep* **11**, 19675 (2021).
- 936 61. Dekeirsschieter, J., Stefanuto, P.-H., Brasseur, C., Haubruge, E. & Focant, J.-F.
937 Enhanced Characterization of the Smell of Death by Comprehensive Two-
938 Dimensional Gas Chromatography-Time-of-Flight Mass Spectrometry
939 (GCxGC-TOFMS). *PLoS One* **7**, e39005 (2012).
- 940 62. Buczynski, M. W. & Parsons, L. H. Quantification of brain endocannabinoid
941 levels: methods, interpretations and pitfalls. *Br J Pharmacol* **160**, 423–442
942 (2010).
- 943 63. Narayanan, M. P., Kannan, V., Vinayan, K. P. & Vasudevan, D. M. Diagnosis
944 of Major Organic Acidurias in Children: Two Years Experience at a Tertiary
945 Care Centre. *Indian Journal of Clinical Biochemistry* **26**, 347–353 (2011).
- 946 64. McMaster, C. R. From yeast to humans – roles of the Kennedy pathway for
947 phosphatidylcholine synthesis. *FEBS Lett* **592**, 1256–1272 (2018).
- 948 65. Law, S.-H. *et al.* An Updated Review of Lysophosphatidylcholine Metabolism
949 in Human Diseases. *Int J Mol Sci* **20**, 1149 (2019).
- 950 66. Falkenburger, B. H., Jensen, J. B., Dickson, E. J., Suh, B.-C. & Hille, B.
951 Phosphoinositides: lipid regulators of membrane proteins modulation of K⁺
952 and Ca²⁺ channels by PIP₂. He discovered PIP₂ regulation of KCNQ
953 channels. *The Authors. Journal compilation C* **588**, 3179–3185 (2010).
- 954 67. Alhouayek, M., Masquelier, J. & Muccioli, G. G. Lysophosphatidylinositols,
955 from Cell Membrane Constituents to GPR55 Ligands. *Trends Pharmacol Sci*
956 **39**, 586–604 (2018).
- 957 68. Smith, P. R. & Wilson, M. T. Detection of haemoglobin in human skeletal
958 remains by ELISA. *J Archaeol Sci* **17**, 255–268 (1990).
- 959 69. Ramsthaler, F., Ebach, S. C., Birngruber, C. G. & Verhoff, M. A. Postmortem
960 interval of skeletal remains through the detection of intraosseal hemin traces. A

- 961 comparison of UV-fluorescence, luminol, Hexagon-OBTI®, and Combur®
962 tests. *Forensic Sci Int* **209**, 59–63 (2011).
- 963 70. Wiley, J., Creamer, J. I. & Buck, A. M. The assaying of haemoglobin using
964 luminol chemiluminescence and its application to the dating of human skeletal
965 remains The assaying of haemoglobin using luminol chemiluminescence.
966 *Luminescence* **24**, 311–316 (2009).
- 967 71. Hervé, M. R., Nicolè, F. & Lê Cao, K. A. Multivariate Analysis of Multiple
968 Datasets: a Practical Guide for Chemical Ecology. *Journal of Chemical Ecology*
969 vol. 44 215–234 Preprint at <https://doi.org/10.1007/s10886-018-0932-6> (2018).
- 970 72. Sud, M. *et al.* Metabolomics Workbench: An international repository for
971 metabolomics data and metadata, metabolite standards, protocols, tutorials and
972 training, and analysis tools. *Nucleic Acids Res* **44**, (2015).
- 973

974

975 **Supplementary figures**

976

977 **Figure 1 – figure supplement 1.** Clustered image map (cim), sample plot and boxplot for the
978 metabolomics data.

979

980 **Figure 1 – figure supplement 2.** Clustered image map (cim) and B) sample plot for the
981 lipidomics data.

982

983 **Figure 1 – figure supplement 3.** Clustered image map (cim), sample plot and boxplot for the
984 proteomics data.

985

986 **Figure 1 – figure supplement 4.** Balanced error variations across variable selection steps.

987

988 **Figure 1 – figure supplement 5.** Score plots for PLS-DA results of all the omics blocks
989 considered.

990

991 **Figure 4 – figure supplement 1.** Flow chart of the experimental design of the study.

992

993 **Supplementary file**

994

995 **Supplementary File 1.** Univariate analyses for all the individual omics.

996

997 **Supplementary File 2.** Environmental data.

998

999 **Source Code File 1.** R pipeline employed in the study.

1000